

Microrod Optical Frequency Reference in the Ambient Environment

Wei Zhang^{1D,*}, Fred Baynes^{1D,†}, Scott A. Diddams^{1D}, and Scott B. Papp^{1D,†}

National Institute of Standards and Technology, 325 Broadway, Boulder, Colorado 80305, USA



(Received 7 March 2019; revised manuscript received 17 June 2019; published 6 August 2019)

We present an ultrahigh- Q , solid-silica microrod resonator operated under ambient conditions that supports laser-fractional-frequency stabilization to the thermal-noise limit of 3×10^{-13} and a linewidth of 62 Hz. We characterize the technical-noise mechanisms for laser stabilization, which contribute significantly less than thermal noise. With fiber photonics, we generate optical and microwave reference signals provided by the microrod modes and the free-spectral range, respectively. Our results suggest the future physical considerations for a miniature, low noise, and robust optical-frequency source.

DOI: 10.1103/PhysRevApplied.12.024010

I. INTRODUCTION

Frequency-stabilized lasers based on detailed designs to mitigate ambient fluctuations have been widely developed to reach new limits of laser linewidth and enhance measurement precision. Evacuated, athermalized, vibration-isolated, and technical-noise-mitigated Fabry-Perot cavities define the state of the art of frequency stability across the optical and microwave domains [1,2]. These ultrastable lasers are critical scientific instruments for precision measurement science, such as atomic optical clocks [3,4], gravitational wave detection [5], very long baseline interferometry [6], and other fundamental and applied research directions. An area of growing interest is to leverage the precision of optical cavities in challenging environments for geodesy [7], transportable optical lattice clock [8], and space-based fundamental physics tests [9,10], which will be enabled by miniature, robust, and portable optical references [11–14].

Whispering-gallery-mode resonators have also been studied for laser-frequency stabilization. In this case, since light is stored inside the material of the resonator, it has been more challenging to implement designs that mitigate ambient fluctuations. In miniature optical-frequency references based on whispering-gallery modes work has focused on fluoride crystals [15–19] that offer exceptionally high optical quality factors of $Q \sim 10^{12}$. Previous research reveals that the fractional frequency stability (FFS) of a laser stabilized to crystals can reach 6×10^{-14} [16], which requires complex ambient isolation, such as a vacuum chamber, multilayer temperature control, and vibration isolation. Understanding the thermal-noise

contribution in these devices has long been an important goal of analytical [19–21] and experimental work [16,19].

Fused-silica microrod resonators [22–24] offer attractive properties, such as a solid monolithic structure, small optical mode volume, and use of silica material and fabrication properties. Though an alternative solution is a chip-based device, such as a high- Q resonator based on a spiral form [25] or external cavity semiconductor laser [26].

Here we report an optical- and microwave-frequency reference by frequency stabilization of a 1551-nm laser to a microrod resonator. The microrod is held in a heated aluminum enclosure with temperature control, but without vacuum or vibration isolation. After characterizing all technical-noise sources in this stable laser system, we demonstrate that the fractional frequency stability reaches the thermal-noise floor at 3×10^{-13} and the laser linewidth is 62 Hz. The thermorefractive (index of refraction) effect is the largest contribution. Furthermore, we generate an 11.8-GHz microwave signal by optical-to-microwave conversion based on stabilization to the microrod's free-spectral range (FSR); this microwave-generation procedure preserves the fractional optical-frequency stability of the microrod for measurement intervals between 100 and 10 000 s. Through experiments and theoretical analysis, our work explores the origins of fluctuations and lays out future physical design directions in whispering-gallery resonators like microrods.

II. EXPERIMENT

The microrod is made of fused silica with a diameter of 6 mm. The resonator [Fig. 1(a) inset] with an unloaded Q factor of 750 million is formed by CO₂ laser machining [22,23]. As shown in Fig. 1(a), the microrod is held by a block of teflon, which is screwed on an aluminum plate ($10 \times 10 \text{ cm}^2$). The laser is coupled into the microrod by a tapered fiber glued on a U-shape mount, which

*wei.zhang@nist.gov

†papp@colorado.edu

[‡]Present address: School of Physical Sciences, The University of Adelaide, Adelaide, Australia.

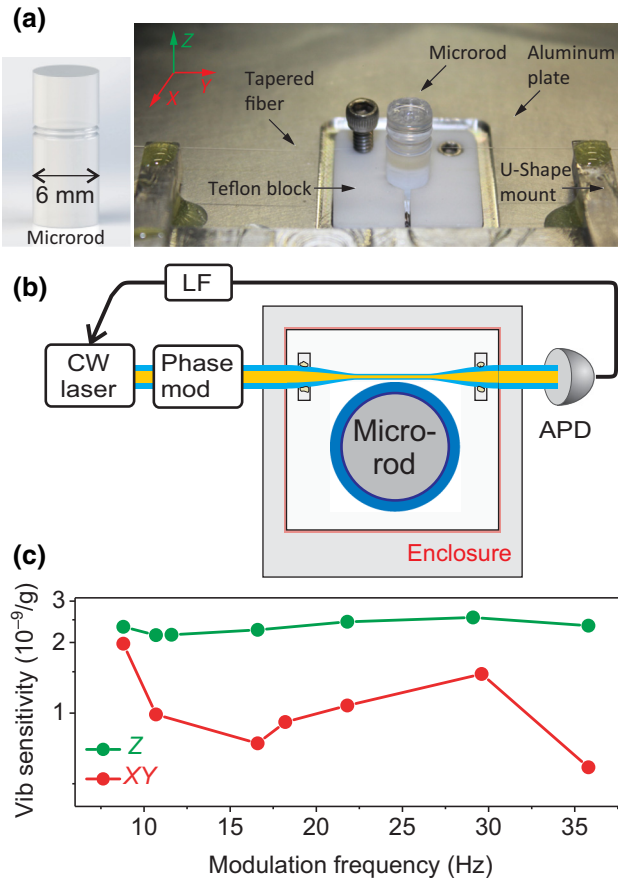


FIG. 1. (a) Photo of the microrod and the tapered fiber coupling. Inset: drawing of the microrod. (b) Schematic of the micro-rod system and photonics components for laser stabilization. CW laser: continuous-wave laser; Phase mod: phase modulation; APD: avalanche photodetector; LF: loop filter. (c) Measurements of the fractional microrod resonance-frequency vibration sensitivity.

is temporarily bolted on a translation stage. In construction of the setup, we perform a one-time adjustment of the tapered-fiber position for near-critical coupling. After this optimization, the U shape is released from the translation stage and glued on the aluminum plate. We attach a thermometer to the aluminum lid and wrap a heat tape on the aluminum enclosure to form a simple temperature-stabilized environment for the microrod.

As shown in Fig. 1(b), an external cavity diode continuous-wave laser at 1551 nm is frequency locked to the microrod with a Pound-Drever-Hall (PDH) locking scheme [27]. We use a fiber-based waveguide electro-optic modulator (EOM) that provides a phase modulation at 8.1 MHz. By using a polarization-maintaining fiber coupler, 10% of the EOM output power is coupled to a photodetector (PD) for residual amplitude modulation (RAM) detection [28,29]. The 90% fiber coupler port, after an inline isolator, is coupled into the microrod by a tapered fiber with a 60% coupling efficiency. The transmission of the

microrod is received by an avalanche photodetector (APD) to generate the PDH error signal by which the laser current modulation port is driven for a frequency lock; the feedback bandwidth is 500 kHz. In the entire setup, all components are either fiber-based devices or compatible with fiber in and output ports, allowing for a compact and robust system. We primarily characterize the microrod-stabilized laser by forming an optical heterodyne beatnote with a laser stabilized to a typical ultralow-expansion cavity [30]. The frequency drift and noise of this beat signal are almost exclusively attributed to the microrod system.

A focus of this paper is characterization of how the microrod-stabilized laser reacts to ambient conditions. One primary concern is vibration noise transferred to the microrod, which leads to deformation [31] and fluctuation of the resonance frequency. Since we do not use any passive or active vibration isolation, we rely on a low vibration sensitivity. Moreover, the vibration sensitivity of microresonator optical references has not been considered extensively, contrary to the case of Fabry-Perot cavities. To measure the vibration sensitivity, the microrod package is placed on an active isolation table, which is driven by the modulation signal from a vector signal analyzer. An accelerometer calibrates the motion of the isolation table and heterodyne beatnote is recorded for frequency response. The fractional frequency vibration sensitivity of the microrod is measured to be $2 \times 10^{-9}/g$ ($g = 9.8 \text{ m/s}^2$) along the gravitational direction and $1 \times 10^{-9}/g$ on the horizontal plane; see Fig. 1(c). To analyze our data, we perform finite-element analysis, which shows the cavity vibration sensitivity is between $3 \times 10^{-10}/g$ along the gravitational and $9 \times 10^{-10}/g$ on the horizontal plane. The difference between measurement and simulation is due to uncertainty in the geometry of the cavity and the cavity mounting. Note this microrod is an approximately cylinder shape, and our achieved vibration sensitivity relies on the small volume rather than vibration-immune design. When the whole system is resting on a fixed optical table, the ambient vibration is measured by an accelerometer placed on top of the microrod package.

III. OPTICAL FREQUENCY NOISE

Now we consider the optical-frequency noise of the microrod-stabilized laser, which is presented by the black “line a” in Fig. 2(a) along with a prediction of the thermorefractive-noise contribution (red “line b”). Our microrod laser is thermal noise limited over decades in Fourier frequency, enabling a relatively narrow integrated linewidth. To understand this behavior, here we use a thermal model for silica material parameterized by the thermal-response time of the microrod. By solving the heat equation for a box and calculating the power-spectral density via the Wiener-Khinchin theorem, we find the

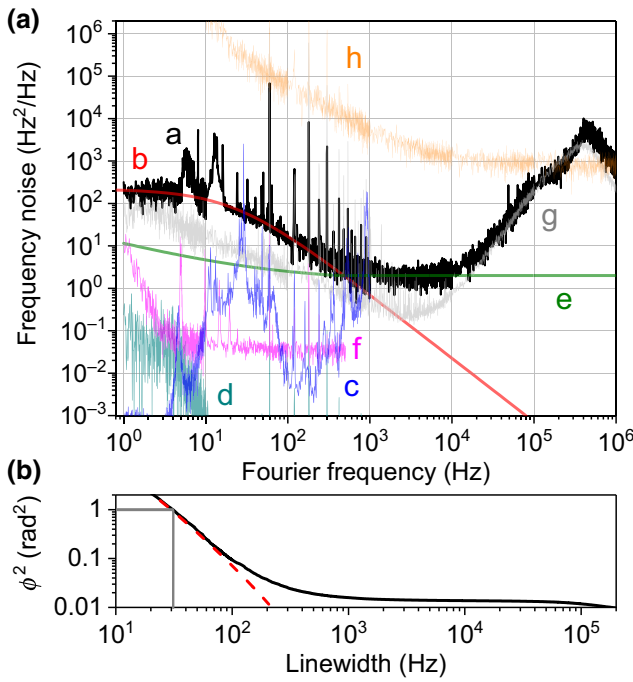


FIG. 2. (a) Frequency-noise power spectral density of microrod-stabilized laser and its noise contributions: “a” the frequency noise of the heterodyne signal between the microrod laser and the reference laser; “b” predicted thermal noise that dominates from 1 Hz to 300 Hz; “c” vibration-induced frequency noise; “d” intensity-induced frequency noise; “e” PDH detector noise including shot noise and detector impedance noise; “f” RAM-induced frequency noise; “g” servo inloop error. “h” the frequency noise of the free-running laser. (b) Integrated phase noise up to 1 rad² leads to the laser linewidth of 62 Hz (black) and the limit due to thermal-noise floor (red).

expression $S_{v_M} \propto v_M^2 \alpha_n^2 / (\omega^2 + \tau_i^{-2})$, where τ_i is the thermal time constant associated with the series of microrod thermal modes, v_M is the optical frequency of a microrod mode, ω is angular frequency, and α_n is the thermorefractive coefficient. Following the important insight of Ref. [19], summation of all the thermal modes yields the power-law relationship $S_{v_M} \propto v_M^2 \alpha_n^2 / [1 + (\omega \tau_T)^{1.5}]$. We normalize this expression to $\langle \delta T^2 \rangle = k_B T^2 / \rho C V$, where δT is the temperature fluctuation associated with the heat capacity C , density ρ , and volume V of the microrod’s optical mode, and T is the ambient temperature [20]. We measure the microrod’s thermal time constant $\tau_T \approx 0.01$ s by frequency-dependent heating the device with our laser. Our measurements establish the thermal-noise floor of microrod references and the path to improvements according to the straightforward formulas above.

We characterize other types of technical noise to understand how the microrod-stabilized laser behaves in ambient conditions. By scaling the vibration power spectrum, which we measure on top of the microrod package, with the measured vibration sensitivity described in Sec. II, the

vibration-induced frequency noise [12,31] is estimated and shown in Fig. 2(a) “line c,” which is below the predicted thermal noise (“line b”) up to 400 Hz. The power fluctuation of the circulating light trapped in the microrod induces cavity resonance-frequency fluctuation mainly due to light absorption. To measure the transfer function from laser intensity to frequency, we modulate the laser power, which is recorded by the APD shown in Fig. 1(b) and heterodyne beatnote is measured for frequency response. This transfer function is 60 kHz/μW at 1 Hz and 6 kHz/μW above 100 Hz. When the laser is frequency locked to the microrod, the intensity-induced frequency noise can be estimated according to the laser intensity noise measured by the APD. We can apply a servo to stabilize the laser power and reduce the intensity-induced frequency noise; alternatively we lower the laser power to 1 μW at which microrod local heating is substantially reduced. As shown in Fig. 2(a) “line d,” the intensity-induced frequency noise is below the predicted thermal-noise floor. The use of low laser power elevates the contribution of the PDH detector noise (“line e”). Since the microrod has a relatively large cavity linewidth, RAM-induced frequency noise should be more substantial in which one part-per-million RAM corresponds to 0.8 Hz frequency fluctuation. The RAM-induced frequency noise [Fig. 2(a) “line f”] is suppressed below the thermal-noise floor by inserting in-line isolation in the system and stabilizing the temperature of the EOM.

A primary concern is ambient-temperature fluctuations or drift that induce microrod frequency fluctuations. The microrod’s thermal isolation is made of the aluminum plate and the teflon block shown in Fig. 1(a). By applying a step change of the temperature on the enclosure and monitoring the laser-frequency change, the time constant is measured to be approximately 1 min. To estimate the temperature-induced frequency fluctuation on the microrod, the temperature fluctuation on the enclosure is multiplied with the transfer function from the enclosure to the microrod. Ambient temperature does not contribute significantly to the frequency-noise power spectrum, but we consider this effect in more detail below.

Besides the ambient environment, technical limitations of the microrod’s Q factor and PDH detection are important to consider. Below 300-Hz Fourier frequency, the frequency noise is dominated by the predicted thermal-noise floor of the microrod. However, from 300 Hz to 10 kHz, shot noise and impedance noise of the APD shown as “line e” are the limit. “Line g” shows the bump from PDH servo above 10 kHz. At lower Fourier frequency, improving the inloop error requires a higher Q resonator. Comparing to the frequency noise when laser is free running (“line h”), the microrod stabilization has an improvement by 10^4 to the inloop level. The vibrations, laser intensity, and RAM shown in Fig. 2(a) are optimized and are not the main limitation.

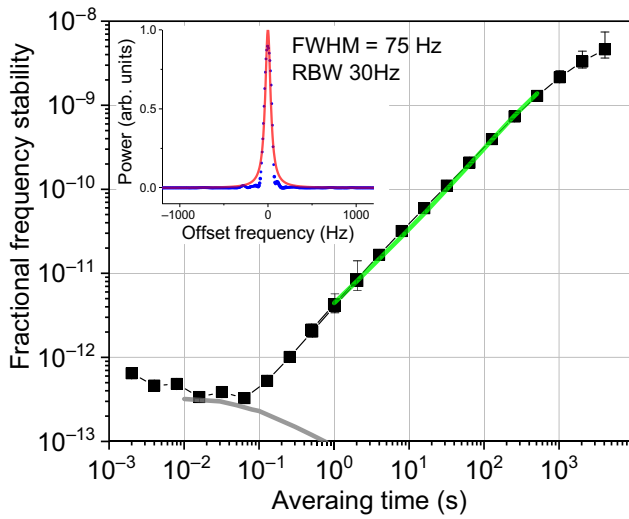


FIG. 3. FFS of the microrod-stabilized laser (black-square line), the thermal-noise floor (gray), and the temperature-induced noise (green). Inset: the measured linewidth of the heterodyne signal (blue dots) representing the microrod-stabilized laser and the Lorentzian fit (red).

One manner to summarize the noise of the microrod-stabilized laser is the integrated phase noise from “line a” in Fig. 2(a). The Fourier frequency equivalent to 1 rad² corresponds to a full-width at half-maximum (FWHM) linewidth of 62 Hz [32], as shown in Fig. 2(b). This linewidth is consistent with the calculation according to the thermal-noise floor of “line b” in Fig. 2(a).

We also characterize the microrod-stabilized laser by an Allan-deviation analysis. We measure the heterodyne signal frequency with a triangle-type, dead-time-free frequency counter and calculate the Allan deviation. We use counter gate times of 2 and 500 ms to increase the dynamic range. As shown in Fig. 3, for averaging time $0.01 \text{ s} < \tau < 0.1 \text{ s}$, the FFS reaches the thermal-noise floor (gray line) at 3×10^{-13} . For $\tau > 1 \text{ s}$, the FFS increases due to frequency drift caused by temperature fluctuations on the enclosure. Moreover, the FWHM linewidth of the heterodyne signal (inset of Fig. 3) as determined with an rf spectrum analyzer is 75 Hz (Lorentz fit, 30-Hz resolution bandwidth), which is fully consistent with frequency noise and Allan deviation results.

IV. LOW-PHASE-NOISE MICROWAVE GENERATION

With the optical-frequency noise properties of the microrod-stabilized laser established, we turn to generating a low-phase-noise microrod-stabilized oscillator. Here the concept is to stabilize a microwave oscillator to the 11.8-GHz FSR, using our laser and PDH locking. The optical frequency of the microrod mode is intrinsically linked by momentum conservation to the FSR through

$v_M = v_{\text{FSR}} \times M$, although the FSR is sensitive to myriad physical parameters, including wavelength, temperature, pressure, resonator shape, index of refraction, and electromagnetic fields. We are interested to explore the phase noise, lower bounded by $S_{v_{\text{FSR}}} = S_{v_M}/M^2$, and the Allan deviation, lower-bounded by $\delta(v_{\text{FSR}})/v_{\text{FSR}} = \delta(v_M)/v_M$ of a microwave oscillator that is locked to the FSR, where $\delta()$ indicates the fluctuations of the quantity [33]. In these limits the microwave oscillator would offer the same FFS as our microrod-stabilized laser. For stabilization to the microrod FSR, we use an optical comb $v_n = v_0 + n f_m$, generated from our laser frequency v_0 and a phase modulator driven by an oscillator at f_m . The laser and comb mode n are PDH locked to respective microrod modes belonging to the same family; the inloop errors of these locks are S_{v_0} and S_{v_n} , respectively [34]. Therefore, we can approximate the microwave oscillator noise as $S_{f_m} = S_{v_{\text{FSR}}} + (S_{v_0} + S_{v_n})/n^2$.

In experiments, 10% laser-power output at frequency of v_0 is locked to the microrod by PDH based on the schematic shown in Fig. 1(b), and 90% is sent to a phase modulator, driven by a microwave synthesizer, to generate comb lines at v_n ; see Fig. 4(a). We choose f_m at 11.8 GHz, and the $n = 37$ comb line is locked to the microrod simultaneously by the second PDH in which the frequency-modulation port of the microwave synthesizer is used as the actuator. Frequency multiplication also facilitates locking the synthesizer. After the two comb modes are locked to the one cavity, the microrod-stabilized oscillator is measured by comparing with a reference microwave synthesizer (Agilent E8257), which is locked to a hydrogen maser. A phase-noise analyzer and frequency counter are used for the comparison.

The black trace in Fig. 4(b) shows the phase noise of the 11.8-GHz microrod-stabilized oscillator, which is -40 dBc/Hz at 10 Hz, -70 dBc/Hz at 100 Hz, and -120 dBc/Hz up to 1 MHz. The data is largely explained by the inloop errors S_{v_0}/n^2 (green trace) and S_{v_n}/n^2 (gray trace). This level of performance is somewhat comparable to other compact oscillators, at the present level of development of our microrod system. We compare a few oscillator technologies in Fig. 4(b): The green-dashed trace shows the phase noise of a high-performance dielectric-resonator oscillator [35], which is as large as 20 dB higher than the microrod-stabilized oscillator. The blue-dashed trace shows results based on frequency division of a Brillouin laser [36], which offers comparable performance. The phase noise of a quartz-based oscillator [37] outperforms the current version of our microrod system by approximately 20 dB; see the orange-dashed trace. Comparing the microrod-stabilized laser at optical frequencies (red trace) to the microrod-stabilized oscillator shows phase noise that is reduced by slightly more than $20 \log(37)$ at some Fourier frequencies, as we would expect from S_{f_m} when the inloop error terms are insignificant.

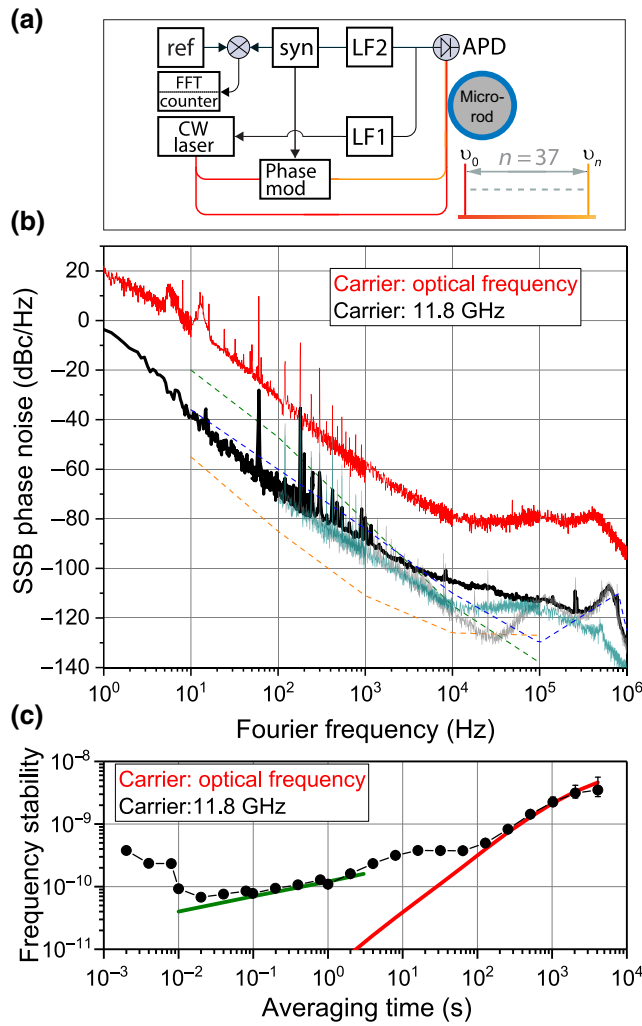


FIG. 4. (a) Schematic of the microrod-stabilized microwave oscillator. CW laser, continuous-wave laser; Phase mod., phase modulator; APD, avalanche photodetector; syn, microwave synthesizer; LF, loop filter; ref, reference microwave synthesizer; FFT, fast Fourier transform analyzer. ν_0 , the laser frequency. ν_n the frequency of the n th comb line. The phase modulators for the two PDH locking systems are not shown. (b) Phase noise of the 11.8-GHz microrod-oscillator (black) is lower than the microrod-stabilized laser (red), and is predominantly limited by inloop errors (green and gray) of the PDH locks. Below 30 Hz, the data is converted from a time-domain measurement. For comparison, a dielectric-resonator oscillator [35] (green dashed), frequency division of a Brillouin laser [36] (blue dashed), and a quartz-based oscillator [37] (orange dashed) are presented. (c) FFS of the microrod oscillator (black), compared with the inloop errors (green) and the FFS of the microrod laser (red).

The solid points (red trace) in Fig. 4(c) show the measured FFS of the microrod-stabilized oscillator (laser). These data are acquired with zero-dead-time frequency-counter measurements and Allan deviation analysis. While the oscillator FFS is limited by the previously described inloop error (green trace) in the millisecond range, for

measurement intervals between 100 and 10 000 s, the FFS is comparable in the microwave and optical domains. We expect this behavior given the link $\nu_M = \nu_{\text{FSR}} \times M$, and we can observe it due to microrod drift. Apparently, other fluctuations of the ambient environment are insignificant in this timescale.

V. CONCLUSION

We demonstrate an optical-frequency reference in the ambient environment based on a microrod-stabilized laser with a FFS at the thermal-noise limit of 3×10^{-13} . We characterize the technical noises, which are below the thermal noise. The long-term stability is dominated by temperature instability, which can be optimized by referencing the laser to an atomic transition in a microfabricated rubidium cell [38]. Furthermore, we show that microrod optical stabilization may also be applied for microwave-signal generation. Our 11.8-GHz microrod-stabilized oscillator provides competitive overall performance in comparison to other compact oscillators mentioned above, and it explores the relative physical influences of optical resonances and the FSR. Note that the phase-coherent frequency division factor used in our experiments is only 37, owing to the limited frequency span of the electro-optic comb. Therefore, the phase noise of our oscillator is primarily limited by electronic noise of the two PDH-locking systems. Either a broader span comb or a narrower linewidth resonator would likely reduce the impact of this effect. The microrod-stabilized laser provides a miniaturized optical- and microwave-frequency reference in an ambient environment, which can benefit field applications such as communications [39], LIDAR [40], and timing distribution and synchronization [41].

ACKNOWLEDGMENTS

We thank D. Nicolodi and L. Stern for their comments. This work was supported by the NIST on a Chip and DARPA PULSE programs. NIST does not seek copyright of this work. Product names are given for information only.

- [1] D. G. Matei, T. Legero, S. Häfner, C. Grebing, R. Weyrich, W. Zhang, L. Sonderhouse, J. M. Robinson, J. Ye, F. Riehle, and U. Sterr, 1.5 μm Lasers with Sub-10 mHz Linewidth, *Phys. Rev. Lett.* **118**, 263202 (2017).
- [2] T. Fortier, M. S. Kirchner, F. Quinlan, J. Taylor, J. C. Bergquist, T. Rosenband, N. Lemke, A. Ludlow, Y. Y. Jiang, C. W. Oates, and S. A. Diddams, Generation of ultrastable microwaves via optical frequency division, *Nat. Photonics* **5**, 425 (2011).
- [3] B. J. Bloom, T. L. Nicholson, J. R. Williams, S. L. Campbell, M. Bishof, X. Zhang, W. Zhang, S. L. Bromley, and J. Ye, An optical lattice clock with accuracy and stability at the 10^{-18} level, *Nature* **506**, 71 (2014).

- [4] N. Hinkley, J. A. Sherman, N. B. Phillips, M. Schioppo, N. D. Lemke, K. Beloy, M. Pizzocaro, C. W. Oates, and A. D. Ludlow, An atomic clock with 10^{-18} instability, *Science* **341**, 1215 (2013).
- [5] R. X. Adhikari, Gravitational radiation detection with laser interferometry, *Rev. Mod. Phys.* **86**, 121 (2014).
- [6] S. Doeleman, T. Mai, A. E. E. Rogers, J. G. Hartnett, M. E. Tobar, and N. Nand, Adapting a cryogenic sapphire oscillator for very long baseline interferometry, *Publ. Astron. Soc. Pac.* **123**, 582 (2011).
- [7] B. D. Tapley, S. Bettadpur, J. C. Ries, P. F. Thompson, and M. M. Watkins, Grace measurements of mass variability in the earth system, *Science* **305**, 503 (2004).
- [8] S. B. Koller, J. Grotti, St. Vogt, A. Al-Masoudi, S. Dörscher, S. Häfner, U. Sterr, and Ch. Lisdat, Transportable Optical Lattice Clock with 7×10^{-17} , *Phys. Rev. Lett.* **118**, 073601 (2017).
- [9] L. Cacciapuoti and Ch. Salomon, Space clocks and fundamental tests: The ACES experiment, *Eur. Phys. J. Spec. Top.* **172**, 57 (2009).
- [10] S. Kolkowitz, I. Pikovski, N. Langellier, M. D. Lukin, R. L. Walsworth, and J. Ye, Gravitational wave detection with optical lattice atomic clocks, *Phys. Rev. D* **94**, 124043 (2016).
- [11] A. D. Ludlow, X. Huang, M. Notcutt, T. Zanon-Willette, S. M. Foreman, M. M. Boyd, S. Blatt, and J. Ye, Compact, thermal-noise-limited optical cavity for diode laser stabilization at 1×10^{-15} , *Opt. Lett.* **32**, 641 (2007).
- [12] J. Millo, D. V. Magalhães, C. Mandache, Y. Le Coq, E. M. L. English, P. G. Westergaard, J. Lodewyck, S. Bize, P. Lemonde, and G. Santarelli, Ultrastable lasers based on vibration insensitive cavities, *Phys. Rev. A* **79**, 053829 (2009).
- [13] S. A. Webster, M. Oxborrow, and P. Gill, Vibration insensitive optical cavity, *Phys. Rev. A* **75**, 011801(R) (2007).
- [14] D. R. Leibrandt, M. J. Thorpe, J. C. Bergquist, and T. Rosenband, Field-test of a robust, portable, frequency-stable laser, *Opt. Express* **19**, 10278 (2011).
- [15] A. A. Savchenkov, A. B. Matsko, V. S. Ilchenko, N. Yu, and L. Maleki, Whispering-gallery-mode resonators as frequency references. II. Stabilization, *J. Opt. Soc. Am. B* **24**, 2988 (2007).
- [16] J. Alnis, A. Schliesser, C. Y. Wang, J. Hofer, T. J. Kippenberg, and T. W. Hänsch, Thermal-noise-limited crystalline whispering-gallery-mode resonator for laser stabilization, *Phys. Rev. A* **84**, 011804(R) (2011).
- [17] I. Fescenko, J. Alnis, A. Schliesser, C. Y. Wang, T. J. Kippenberg, and T. W. Hänsch, Dual-mode temperature compensation technique for laser stabilization to a crystalline whispering gallery mode resonator, *Opt. Express* **20**, 19185 (2012).
- [18] L. M. Baumgartel, R. J. Thompson, and N. Yu, Frequency stability of a dual-mode whispering gallery mode optical reference cavity, *Opt. Express* **20**, 29798 (2012).
- [19] J. Lim, A. A. Savchenkov, E. Dale, W. Liang, D. Eliyahu, V. Ilchenko, A. B. Matsko, L. Maleki, and C. W. Wong, Chasing the thermodynamical noise limit in whispering-gallery-mode resonators for ultrastable laser frequency stabilization, *Nat. Commun.* **8**, 8 (2017).
- [20] A. B. Matsko, A. A. Savchenkov, N. Yu, and L. Maleki, Whispering-gallery-mode resonators as frequency references. I. Fundamental limitations, *J. Opt. Soc. Am. B* **24**, 1324 (2007).
- [21] M. L. Gorodetsky and I. S. Grudinin, Fundamental thermal fluctuations in microspheres, *J. Opt. Soc. Am. B* **21**, 697 (2004).
- [22] S. B. Papp, P. Del'Haye, and S. A. Diddams, Mechanical Control of a Microrod-resonator Optical Frequency Comb, *Phys. Rev. X* **3**, 031003 (2013).
- [23] P. Del'Haye, S. A. Diddams, and S. B. Papp, Laser-machined ultra-high- Q microrod resonators for nonlinear optics, *Appl. Phys. Lett.* **102**, 221119 (2013).
- [24] W. Loh, A. A. S. Green, F. N. Baynes, D. C. Cole, F. Quinlan, H. Lee, K. J. Vahala, S. B. Papp, and S. A. Diddams, Dual-microcavity narrow-linewidth Brillouin laser, *Optica* **2**, 225 (2015).
- [25] H. Lee, M.-G. Suh, T. Chen, J. Li, S. A. Diddams, and K. J. Vahala, Spiral resonators for on-chip laser frequency stabilization, *Nat. Commun.* **4**, 2468 (2013).
- [26] W. Liang, V. S. Ilchenko, D. Eliyahu, A. A. Savchenkov, A. B. Matsko, D. Seidel, and L. Maleki, Ultralow noise miniature external cavity semiconductor laser, *Nat. Commun.* **6**, 7371 (2015).
- [27] R. W. P. Drever, J. L. Hall, F. V. Kowalski, J. Hough, G. M. Ford, A. J. Munley, and H. Ward, Laser phase and frequency stabilization using an optical resonator, *Appl. Phys. B* **31**, 97 (1983).
- [28] N. C. Wong and J. L. Hall, Servo control of amplitude modulation in frequency-modulation spectroscopy: demonstration of shot-noise-limited detection, *J. Opt. Soc. Am. B* **2**, 1527 (1985).
- [29] W. Zhang, M. J. Martin, C. Benko, J. L. Hall, J. Ye, C. Hagemann, T. Legero, U. Sterr, F. Riehle, G. D. Cole, and M. Aspelmeyer, Reduction of residual amplitude modulation to 1×10^{-6} for frequency modulation and laser stabilization, *Opt. Lett.* **39**, 1980 (2014).
- [30] F. N. Baynes, F. Quinlan, T. Fortier, Q. Zhou, A. Beling, J. C. Campbell, and S. A. Diddams, Attosecond timing in optical-to-electrical conversion, *Optica* **2**, 141 (2015).
- [31] L. Chen, J. L. Hall, J. Ye, T. Yang, E. Zang, and T. Li, Vibration-induced elastic deformation of fabry-perot cavities, *Phys. Rev. A* **74**, 053801 (2006).
- [32] J. L. Hall and M. Zhu, in *Laser Manipulation of Atoms and Ions, Proceedings Internat. School of Physics Enrico Fermi, Vol. Course CXVIII* (North Holland-Elsevier, Amsterdam, 1992), p. 671.
- [33] L. Maleki, A. A. Savchenkov, V. S. Ilchenko, W. Liang, D. Eliyahu, A. B. Matsko, D. Seidel, N. P. Wells, J. C. Campanaro, and B. Jadusziwer, in *2011 Joint Conference of the IEEE International Frequency Control and the European Frequency and Time Forum (FCS) Proceedings* (IEEE, 2011), p. 1.
- [34] W. C. Swann, E. Baumann, F. R. Giorgetta, and N. R. Newbury, Microwave generation with low residual phase noise from a femtosecond fiber laser with an intracavity electro-optic modulator, *Opt. Express* **19**, 24387 (2011).
- [35] <https://synergymwave.com/>.
- [36] J. Li, X. Yi, H. Lee, S. A. Diddams, and K. J. Vahala, Electro-optical frequency division and stable microwave synthesis, *Science* **345**, 309 (2014).

- [37] <http://www.wenzel.com/>.
- [38] W. Loh, M. T. Hummon, H. F. Leopardi, T. Fortier, F. Quinlan, J. Kitching, S. B. Papp, and S. A. Did-dams, Microresonator Brillouin laser stabilization using a microfabricated rubidium cell, *Opt. Express* **24**, 14513 (2016).
- [39] H. Al-Taiy, N. Wenzel, S. Preußler, J. Klinger, and T. Schneider, Ultra-narrow linewidth, stable and tunable laser source for optical communication systems and spectroscopy, *Opt. Lett.* **39**, 5826 (2014).
- [40] I. Coddington, W. C. Swann, L. Nenadovic, and N. R. Newbury, Rapid and precise absolute distance measurements at long range, *Nat. Photonics* **3**, 351 (2009).
- [41] J. Kim, J. A. Cox, J. Chen, and F. X. Kärtner, Drift-free femtosecond timing synchronization of remote optical and microwave sources, *Nat. Photonics* **2**, 733 (2008).